Research Square

Preprints are preliminary reports that have not undergone peer review.
They should not be considered conclusive, used to inform clinical practice,
or referenced by the media as validated information.

FAM155B driven by BPTF promotes breast cancer progression and paclitaxel resistance via SREBP1-mediated fatty acid metabolic reprogramming

Yihong Luo
Zhongshan Hospital
Sijia Zhang
Zhongshan Hospital
Weifeng Qu
Zhongshan Hospital
Xuhui Zhao
Shanghai Medical College, Fudan University
Yuan Fang
Zhongshan Hospital
Jun Gao
Zhongshan Hospital
Jingyi Wang
Zhongshan Hospital
Shiguang Yang
Nanjing Drum Tower Hospital, the Affiliated Hospital of Medical School
Wei Zhu
Zhongshan Hospital
Zhilong Ai
Zhongshan Hospital
Wei Zhang
Huashan Hospital, Fudan University
Zhenyu Zheng
Songyuan Jilin Oilfield Hospital
He Li
li.he@zs-hospital.sh.cn

Zhongshan Hospital

Research Article

Keywords: FAM155B, breast cancer, BPTF, SREBP1, fatty acid metabolism, lipid metabolic reprogramming, paclitaxel resistance

Posted Date: July 21st, 2026

DOI: https://doi.org/10.21203/rs.3.rs-10340968/v1

License: This work is licensed under a Creative Commons Attribution 4.0 International License. Read Full License

Additional Declarations: No competing interests reported.

Abstract

Background

Breast cancer poses a severe global public health burden, where tumor progression, metastasis and chemoresistance substantially compromise therapeutic outcomes. Metabolic reprogramming, particularly aberrant fatty acid metabolism, facilitates malignant transformation and drug resistance. Nevertheless, the key molecular mediators linking lipid remodeling to breast cancer advancement and paclitaxel resistance remain largely uncharacterized.

Methods

We analyzed FAM155B expression and clinical significance via public transcriptomic data and clinical specimens. Gain/loss-of-function assays assessed its roles in tumor growth, metastasis and paclitaxel sensitivity. RNA-seq, qPCR, immunoblotting and BODIPY staining detected lipid metabolic changes, while rescue experiments validated SREBP1 and fatty acid synthesis downstream of FAM155B. Bioinformatics, luciferase and ChIP-qPCR assays confirmed BPTF-mediated transcriptional activation of FAM155B.

Results

The expression level of FAM155B was significantly upregulated in breast cancer tissues and cell lines, and elevated FAM155B expression was closely correlated with advanced clinical stages and unfavorable patient prognosis. Functional validation experiments demonstrated that FAM155B exerts oncogenic effects by facilitating the proliferation, migration, and invasion of breast cancer cells, as well as promoting xenograft tumor growth in vivo. Mechanistically, FAM155B activates the fatty acid biosynthesis program, leading to increased free fatty acids and lipid droplet accumulation. Further mechanistic investigations identified SREBP1 as a critical downstream mediator responsible for FAM155B-regulated lipid metabolic reprogramming. In addition, the chromatin remodeler BPTF was verified to directly bind to the promoter region of FAM155B, thereby transcriptionally activating FAM155B expression and driving lipid remodeling and malignant progression of breast cancer. Moreover, genetic depletion of FAM155B markedly enhanced the chemosensitivity of breast cancer cells to paclitaxel treatment both in vitro and in vivo.

Conclusions

Collectively, FAM155B drives breast cancer progression and paclitaxel resistance. The BPTF/FAM155B/SREBP1 axis facilitates tumor progression and paclitaxel resistance via fatty acid

metabolic reprogramming, and targeting this cascade holds therapeutic potential to enhance taxane chemotherapy efficacy.

Background

Breast cancer is the most common malignancy and a leading cause of cancer-related mortality among women worldwide [1–3]. Despite advances in screening, molecular classification, and multimodal treatments—such as targeted therapy, immunotherapy, and chemotherapy—metastasis and therapeutic resistance remain major causes of clinical failure [4].

Paclitaxel is a first-line taxane agent used in breast cancer treatment, which works by stabilizing microtubules and inducing mitotic arrest [5, 6]. However, intrinsic or acquired resistance often limits its efficacy. The mechanisms underlying paclitaxel resistance are complex, involving inflammatory signaling, anti-apoptotic remodeling, mitochondrial stress, and epigenetic alterations [7–10]. Recently, metabolic plasticity has been recognized as another crucial factor in chemoresistance. Nevertheless, the molecular pathways linking oncogenic signaling, metabolic adaptation, and paclitaxel resistance remain unclear.

Metabolic reprogramming enables tumor cells to sustain rapid proliferation and adapt to environmental stress, establishing itself as a core hallmark of cancer [11, 12]. While the Warburg effect is well-documented [13], cancer cells also flexibly rewire other networks according to nutrient availability and therapeutic pressure, including lipid metabolism [14]. Alterations in lipid uptake, storage, and de novo lipogenesis provide the structural components for membrane biogenesis and energy reserves necessary for cancer progression and therapy resistance [15–17]. In breast cancer, elevated lipogenic activity—particularly driven by key enzymes like fatty acid synthase (FASN) [18] and master transcription factors like SREBP1 [19]. —frequently correlates with tumor aggressiveness and oncogenic signal transduction [20].

Family with sequence similarity 155 member B (FAM155B) is a poorly characterized gene, and its biological role in human cancers remains unexplored. Specifically, whether FAM155B integrates with metabolic reprogramming or contributes to chemotherapeutic resistance is unknown. In this study, we investigated the function of FAM155B in breast cancer, revealing an unexpected role for the BPTF/FAM155B/SREBP1 lipogenic axis in driving tumor progression and paclitaxel resistance.

Materials and Methods

Clinical Samples and Data Acquisition

Human breast cancer (BRCA) tissues and matched adjacent normal tissues (n=62) were collected from patients who underwent surgical resection at Zhongshan Hospital, Fudan University. Informed consent was obtained from all patients, and this study was approved by the Institutional Ethics Committee of Zhongshan Hospital, Fudan University (Approval Number: B2024-237). Publicly available gene

expression data and corresponding clinical information for BRCA patients were acquired from The Cancer Genome Atlas (TCGA) dataset and the Gene Expression Omnibus (GEO) database (GSE54002).

Cell Culture and Reagents

Human breast cancer cell lines (MCF-7, SK-BR-3, T-47D, MDA-MB-231) and the normal breast epithelial cell line MCF-10A were purchased from the American Type Culture Collection (ATCC, Manassas, VA, USA). Breast cancer cells were cultured in an appropriate medium (DMEM for MDA-MB-231, T-47D, MCF-7 and SK-BR-3) supplemented with 10% fetal bovine serum (FBS, Gibco, USA) and 1% penicillin/streptomycin at 37°C in a humidified incubator containing 5% CO_2. MCF-10A cells were maintained in DMEM/F12 medium supplemented with 5% horse serum, 20 ng/mL EGF, 0.5 μg/mL hydrocortisone, 100 ng/mL cholera toxin, 10 μg/mL insulin, and 1% penicillin/streptomycin under the same culture conditions. Paclitaxel and the FASN inhibitor FASN-IN-1 were obtained from MedChemExpress (USA).

Plasmid Construction and Cell Transfection

To establish stable knockdown and overexpression cell lines, short hairpin RNAs (shRNAs) targeting FAM155B, SREBP1, or BPTF (shFAM155B-1/2, shSREBP1, shBPTF), small interfering RNAs (siRNAs) targeting BCL6, MYC, or HIF1A, and corresponding overexpression plasmids were synthesized by GenePharma (Shanghai, China). Lentiviral packaging and cell infection were strictly performed following the manufacturer's instructions, and stable clones were selected using puromycin (Solarbio, Beijing, China).

RNA Extraction, RNA-seq, and Quantitative Real-Time PCR (RT-qPCR)

Total RNA was extracted using TRIzol reagent (Invitrogen, Thermo Fisher Scientific, USA). RNA sequencing (RNA-seq) was exclusively performed by Tsingke Biotechnology Co., Ltd. (Shanghai, China), followed by Gene Set Enrichment Analysis (GSEA). For RT-qPCR, total RNA was reverse-transcribed into cDNA using the One-Step qRT-PCR Kit (Novoprotein, China). RT-qPCR was performed using SYBR Green Master Mix (Novoprotein, China) on a CFX96 (Bio-Rad). Relative gene expression was calculated using the $2^{-\Delta\Delta Ct}$ method with ACTIN as the endogenous control, in compliance with the MIQE guidelines. All primer sequences are listed in Supplementary Table S1.

Protein Extraction and Western Blot

Protein Extraction and Western Blot

Total cellular proteins were extracted using RIPA lysis buffer supplemented with a protease inhibitor cocktail (Beyotime, Shanghai, China). Protein concentration was determined using a BCA Protein Assay Kit (Beyotime, China). Equal amounts of proteins were separated by SDS-PAGE and transferred onto PVDF membranes (Millipore, USA). The membranes were incubated overnight with primary antibodies against FAM155B, SREBP1, SREBP2, ChREBP, ACTIN, followed by incubation with HRP-conjugated secondary antibodies. Protein bands were visualized using an ECL detection system (Bio-Rad ChemiDoc MP, USA). Table S2 for detailed antibody information

Metabolic Assays and Lipid Droplet Staining

The relative intracellular levels of total triglycerides (TG) and free fatty acids (FFA) were quantified using commercially available assay kits (Beyotime, Shanghai, China; TG: Cat# S0219S; FFA: Cat# S0215S) according to the standard protocols. For lipid droplet accumulation analysis, cells were stained with BODIPY 493/503 dye (Beyotime, Cat# C2053S, China) and counterstained with DAPI for nuclear visualization. Images were captured utilizing a fluorescence microscope.

In Vitro Cell Phenotype Assays

Cell viability and paclitaxel IC_{50} values were assessed using the Cell Counting Kit-8 (CCK-8) assay (Beyotime, Shanghai, China; Cat# C0037) at predetermined time points (0, 24, 48, 72, and 96 h). Cell proliferation was further evaluated by colony formation assays and EdU incorporation assays using an EdU kit (Beyotime, Cat# C0081S, China). Cell migration was evaluated via wound healing assays, where the relative wound closure area was calculated at 0 and 24 h. Cell invasion capacity was determined using Transwell chambers pre-coated with Matrigel (Corning, USA).

Dual-Luciferase Reporter Assay and ChIP-qPCR

The wild-type (WT) or mutant (MUT) putative BPTF binding sites in the FAM155B promoter region were cloned into luciferase reporter vectors (Beyotime, Shanghai, China). Cells were co-transfected with the reporter plasmids and BPTF overexpression plasmids. Luciferase activities were quantified using a Dual-Luciferase Reporter Assay System (Beyotime, RG027, China). Chromatin immunoprecipitation (ChIP) was conducted using a ChIP assay kit (Beyotime, P2078, China). Chromatin was immunoprecipitated with an anti-BPTF antibody or control IgG, and the enriched DNA fragments encompassing the FAM155B promoter were quantified via qPCR.

In Vivo Tumor Xenograft Model

All animal care and experimental procedures were thoroughly approved by the Animal Care and Use Committee of Zhongshan Hospital, Fudan University and carried out strictly complying with the ARRIVE guidelines. Female BALB/c nude mice (4–6 weeks old, n=5 per group) were purchased from Shanghai

Vital River Laboratory Animal Technology Co., Ltd. (Shanghai, China). MDA-MB-231 cells with or without stable FAM155B knockdown were subcutaneously injected into the flanks of the mice. Tumor volumes were monitored every 5 days (Volume=0.5×Length×Width^2). For the drug resistance model investigation, mice received an intraperitoneal injection of Paclitaxel or vehicle control. The mice were euthanized at day 25, and tumors were excised, weighed, and subjected to histological evaluation.

Histology and Immunohistochemistry (IHC)

Tumor tissues and clinical specimens were fixed in 4% paraformaldehyde, paraffin-embedded, and completely sectioned. Tissue sections were subjected to Hematoxylin and Eosin (HE) staining and immunohistochemistry (IHC) utilizing specific antibodies against FAM155B or Ki67. Staining intensities and the proportion of positive cells were blindly evaluated to determine the final IHC scores.

Statistical Analysis

All statistical analyses were executed using GraphPad Prism 11.0.1 (GraphPad Software, USA) software. Data originating from a minimum of three independent experiments were presented as Mean ± Standard Deviation (SD). Differences between two groups were strictly interpreted utilizing the two-tailed unpaired or paired Student's t-test. For comparisons among multiple groups, one-way analysis of variance (ANOVA) followed by Tukey's post-hoc test or two-way ANOVA was utilized. Survival curves were generated using the Kaplan-Meier method coupled with log-rank tests. Pearson or Spearman correlation coefficients were calculated for gene expression correlation evaluation. A p-value of < 0.05 was considered statistically significant (* p < 0.05, ** p < 0.01, *** p < 0.001).

Results

Upregulation of FAM155B correlates with adverse prognosis in human breast cancer

We initially investigated FAM155B expression profiles in breast cancer (BC) using public datasets. Data from The Cancer Genome Atlas (TCGA) showed that FAM155B mRNA was significantly enriched in BRCA tissues compared with normal breast tissues (Fig. 1A). This upregulation was consistent with the GSE54002 dataset, where FAM155B expression was elevated in tumor samples relative to normal controls (Fig. 1B).

We then analyzed the correlation between FAM155B and clinical features. Although FAM155B expression fluctuated across different molecular subtypes (Fig. 1C), high FAM155B levels clearly correlated with advanced clinical stages (Stage III/IV) and increased 5-year mortality (Fig. 1D). Kaplan-Meier survival analysis further showed that patients with high FAM155B expression experienced poorer disease-free survival (DFS) and overall survival (OS) (Fig. 1E).

To verify the bioinformatics data, we evaluated FAM155B expression in our own cohort. qPCR analysis of 62 paired human BC and adjacent normal tissues (ANTs) revealed a distinct increase of FAM155B mRNA

in tumors (Fig. 1F). At the protein level, Western blotting of six paired samples showed enriched FAM155B in the tumor tissues (Fig. 1G). Similarly, immunohistochemistry (IHC) staining confirmed intense FAM155B signals within BC tissues compared to surrounding non-tumor areas, reflecting higher IHC positive scores (Fig. 1H).

In summary, our data show that FAM155B is overexpressed in breast cancer and associated with malignant progression and poor survival outcomes.

FAM155B significantly promotes the proliferation, invasion, and migration of breast cancer cells in vitro

To advance our understanding of the biological function of FAM155B in BC progression, we performed gain-of-function and loss-of-function experiments *in vitro*. First, we comprehensively screened the endogenous expression of FAM155B across a normal breast epithelial cell line (MCF-10A) and four BC cell lines (MCF-7, SK-BR-3, T-47D, and MDA-MB-231). Both quantitative real-time PCR and Western blot analyses substantiated that FAM155B was elevated in all tested BC cell lines compared to MCF-10A cells, with MDA-MB-231 exhibiting the highest expression and MCF-7 showing relatively lower levels (Fig. 2A, B). Based on these profiles, we utilized short hairpin RNAs (shFAM-1 and shFAM-2) to stably knock down FAM155B in MDA-MB-231 cells, and introduced stable overexpression vectors into MCF-7 cells. The transfection efficiencies were strictly verified at both mRNA and protein levels (Fig. 2C, D).

Next, we assessed the effect of FAM155B on BC cell proliferation. CCK-8 assays revealed that silencing FAM155B significantly suppressed the viability of MDA-MB-231 cells, whereas its exogenous overexpression markedly accelerated the growth trajectory of MCF-7 cells over a 96-hour period (Fig. 2E). Consistently, colony formation assays demonstrated that FAM155B ablation severely impaired the clonogenic ability of MDA-MB-231 cells, while forced expression of FAM155B enhanced it in MCF-7 cells (Fig. 2F). Furthermore, EdU incorporation assays independently confirmed that the proportion of actively synthesized DNA in proliferating cells was dramatically decreased upon FAM155B knockdown but significantly elevated following FAM155B upregulation (Fig. 2G).

Since tumor metastasis is a critical determinant of BC malignancy [12865918], we further evaluated the migratory and invasive capacities utilizing wound healing and Transwell matrix invasion assays, respectively. The empirical data strictly indicated that downregulation of FAM155B profoundly hindered both the invasive cell counts (Fig. 2H) and the relative wound closure rate (Fig. 2I) of MDA-MB-231 cells. Conversely, upregulating FAM155B endowed MCF-7 cells with enhanced invasive and migratory propensities.

Taken together, these *in vitro* functional assays stringently suggest that FAM155B acts as an oncogenic driver that facilitates the proliferation, invasive behaviors, and metastatic potential of breast cancer cells.

Downregulation of FAM155B significantly impedes the growth of breast cancer xenografts in vivo

To determine the functional role of FAM155B in BC, we performed *in vitro* gain- and loss-of-function experiments. We initially examined FAM155B expression across a normal breast epithelial cell line (MCF-

10A) and four BC cell lines. qPCR and Western blotting revealed that FAM155B was elevated in the BC cell lines relative to MCF-10A cells. Given that MDA-MB-231 cells expressed the highest levels of FAM155B and MCF-7 cells the lowest (Fig. 2A, B), we established stable FAM155B knockdown in MDA-MB-231 cells using shRNAs (shFAM-1 and shFAM-2) and stably overexpressed FAM155B in MCF-7 cells. Expression modulation was validated at the mRNA and protein levels (Fig. 2C, D).

Subsequent functional assays focused on cell proliferation. CCK-8 results indicated that FAM155B knockdown impaired the viability of MDA-MB-231 cells, while its overexpression accelerated MCF-7 cell growth (Fig. 2E). Colony formation assays yielded consistent results: silencing FAM155B reduced the number of colonies in MDA-MB-231 cells, whereas FAM155B overexpression increased clonogenicity in MCF-7 cells (Fig. 2F). Furthermore, EdU incorporation analysis confirmed that DNA synthesis was suppressed by FAM155B knockdown and stimulated by its overexpression (Fig. 2G).

To address the impact of FAM155B on tumor metastasis [12865918], we performed wound healing and Transwell invasion assays. The results showed that FAM155B ablation decreased the invasive capacity (Fig. 2H) and delayed wound closure (Fig. 2I) in MDA-MB-231 cells. In contrast, upregulating FAM155B in MCF-7 cells significantly increased their migratory and invasive potential.

Collectively, these findings demonstrate that FAM155B acts as an oncogenic factor that enhances the growth and motility of breast cancer cells.

FAM155B drives breast cancer progression by orchestrating fatty acid metabolic reprogramming

Since metabolic reprogramming is a recognized hallmark of tumor progression [21, 22], we investigated how FAM155B alters the transcriptomic landscape of BC cells. RNA sequencing (RNA-seq) of control and FAM155B-knockdown MDA-MB-231 cells (Figure S1A), combined with KEGG and Gene Set Enrichment Analysis (GSEA), showed a significant enrichment of differentially expressed genes in the "Fatty acid biosynthesis" pathway (Figs. 4A, B). A clustered heatmap further confirmed the downregulation of multiple lipogenic genes following FAM155B silencing (Figure S1B).

We next validated the expression of rate-limiting enzymes involved in de novo fatty acid and triglyceride (TG) synthesis, including ACACA, FASN, SCD1, ACSL3, and DGAT1 (Fig. 4C) [23, 24]. qPCR and Western blot analyses confirmed that FAM155B knockdown decreased the mRNA and protein levels of these enzymes in MDA-MB-231 cells (Figs. 4D, E). Conversely, FAM155B overexpression upregulated these lipogenic enzymes in MCF-7 cells (Fig. 4E, Figure S1C). Furthermore, clinical data analysis revealed a positive correlation between FAM155B and the expression of these genes (Figure S1D, E).

Biochemical analysis showed that FAM155B knockdown reduced the intracellular levels of palmitate, oleate (Fig. 4F), total free fatty acids (FFA), and TG (Fig. 4G) in MDA-MB-231 cells. The opposite trend was observed in FAM155B-overexpressing MCF-7 cells (Figure S1F, G). Because intracellular neutral lipids are stored in lipid droplets (LDs), we utilized BODIPY 493/503 staining. The images indicated that

FAM155B depletion reduced cytosolic LDs in MDA-MB-231 cells (Fig. 4H), whereas its overexpression increased LD accumulation in MCF-7 cells (Figure S1H).

To determine if the oncogenic function of FAM155B depends on fatty acid synthesis, we used a FASN specific inhibitor (FASN-IN-1). Pharmacological blockade of lipid synthesis reversed the enhanced colony formation (Fig. 4I) and invasion (Fig. 4J) induced by FAM155B overexpression.

Together, these data suggest that FAM155B drives malignant behaviors in breast cancer by promoting *de novo* lipogenesis.

FAM155B orchestrates lipid metabolic reprogramming and oncogenic phenotypes by upregulating the transcription factor SREBP1

To identify the downstream effector of FAM155B-induced lipogenesis, we examined the master transcriptional regulators of lipid homeostasis, specifically sterol regulatory element-binding proteins (SREBPs) and carbohydrate-responsive element-binding protein (ChREBP) [25, 26]. qPCR and Western blot analyses showed that manipulating FAM155B expression altered the mRNA and protein levels of SREBP1 in both MDA-MB-231 and MCF-7 cells, while the expression of SREBP2 and ChREBP remained unaffected (Fig. 5A, B). Furthermore, correlation analysis of our clinical tissue cohort (Fig. 5C) and the TCGA database (Figure S2A) demonstrated a significant positive correlation between FAM155B and SREBP1 expression in breast cancer tissues.

To confirm that SREBP1 mediates the downstream lipogenic machinery, we knocked down or overexpressed SREBP1 using specific shRNAs or lentiviral vectors (Figure S2B, C). As expected, SREBP1 silencing downregulated the transcription of the aforementioned rate-limiting enzymes (ACACA, FASN, SCD1, ACSL3, and DGAT1) and reduced the intracellular pools of FFA and TG. Conversely, SREBP1 overexpression promoted these lipid synthesis cascades (Fig. 5D, E).

To establish the functional dependency of the FAM155B/SREBP1 axis, we performed rescue assays by knocking down SREBP1 in FAM155B-overexpressing MCF-7 cells. SREBP1 depletion reversed the excessive intracellular accumulation of TG and FFA (Fig. 5F) and reduced the cytosolic lipid droplet accumulation (Fig. 5G) driven by FAM155B. Moreover, phenotypic rescue assays demonstrated that silencing SREBP1 abolished the enhanced colony formation (Fig. 5H) and invasive capability (Fig. 5I) induced by FAM155B overexpression.

Collectively, these data indicate that SREBP1 is a crucial downstream mediator through which FAM155B executes lipid metabolic reprogramming and promotes oncogenic phenotypes in breast cancer.

The transcription factor BPTF directly targets and upregulates FAM155B to promote lipid metabolism and tumor progression

To determine the upstream mechanism regulating elevated FAM155B expression in breast cancer, we predicted potential transcription factors binding to the FAM155B promoter using three independent databases (JASPAR, PROMO, and GTRD). Intersection of these databases identified four candidates: BCL6, MYC, HIF1A, and BPTF (Fig. 6A). TCGA dataset analysis revealed a significant positive correlation between BPTF and FAM155B expression (Fig. 6B), whereas the other candidates showed no significant correlations (Figure S3A). Consistently, knockdown of BCL6, MYC, or HIF1A did not affect FAM155B expression (Figure S3B, C). In contrast, BPTF knockdown reduced both the mRNA and protein levels of FAM155B in MCF-7 and MDA-MB-231 cells (Fig. 6C), identifying BPTF as a potential upstream regulator.

To determine if BPTF directly transactivates FAM155B, we performed dual-luciferase reporter and ChIP-qPCR assays. Reporter assays showed that BPTF overexpression increased the luciferase activity of the wild-type (WT) FAM155B promoter, an effect that was abolished upon mutation (MUT) of the putative BPTF-binding motif (Fig. 6D). Furthermore, ChIP-qPCR demonstrated significant BPTF enrichment at the endogenous FAM155B promoter relative to the IgG control (Fig. 6E). These results confirm that BPTF transcriptionally upregulates FAM155B via direct promoter binding.

To establish whether BPTF drives lipid reprogramming and oncogenic behaviors in a FAM155B-dependent manner, we performed functional rescue assays. Biochemical and morphological evaluations indicated that BPTF overexpression increased intracellular FFA and TG levels, and promoted cytosolic lipid droplet accumulation. Concurrent depletion of FAM155B reversed these BPTF-induced lipogenic effects (Fig. 6F, G; Figure S3D). Consistent with the metabolic changes, BPTF overexpression enhanced cell viability (Fig. 6H), colony formation (Fig. 6I), and cell invasion (Fig. 6J), all of which were neutralized by FAM155B knockdown.

Collectively, these data demonstrate that BPTF directly transactivates FAM155B, forming a BPTF/FAM155B axis that drives aberrant lipid metabolic reprogramming and breast cancer progression.

FAM155B depletion sensitizes breast cancer cells to paclitaxel treatment

Since metabolic reprogramming is closely associated with therapeutic resistance [27, 28], we examined whether FAM155B affects breast cancer chemoresistance. Gene set enrichment analysis (GSEA) revealed a significant enrichment of drug resistance-related gene signatures in the control group compared to the FAM155B-knockdown group, suggesting a potential association between FAM155B and chemoresistance (Fig. 7A).

To test this, we treated FAM155B-modified breast cancer cells with increasing concentrations of paclitaxel. Dose-response curves indicated that FAM155B knockdown increased the paclitaxel sensitivity of MDA-MB-231 cells, whereas FAM155B overexpression increased resistance in MCF-7 cells. Specifically, FAM155B depletion reduced the half-maximal inhibitory concentration (IC50) of paclitaxel, while its overexpression increased the IC50 value (Fig. 7B).

We next investigated whether FAM155B silencing potentiates the efficacy of paclitaxel *in vitro*. CCK-8 assays demonstrated that while FAM155B knockdown or paclitaxel alone suppressed MDA-MB-231 cell viability, their combination exerted the strongest growth-inhibitory effect over 96 hours (Fig. 7C). Similarly, paclitaxel impaired clonogenic survival, an effect further enhanced by FAM155B depletion (Fig. 7D). Furthermore, FAM155B knockdown combined with paclitaxel suppressed the invasive capacity of MDA-MB-231 cells more effectively than either intervention alone (Fig. 7E).

To validate these findings *in vivo*, we established xenograft models using control and FAM155B-knockdown MDA-MB-231 cells, followed by paclitaxel administration. The combination of FAM155B silencing and paclitaxel resulted in the smallest tumor masses among all groups (Fig. 7F). Tumor volume tracking showed that while monotherapies partially restrained xenograft expansion, the combined intervention provided the most effective tumor suppression (Fig. 7G). Endpoint tumor weights confirmed that FAM155B depletion enhanced paclitaxel-induced tumor inhibition (Fig. 7H). Immunohistochemical staining for Ki67 revealed the lowest proliferative index in the combination group, supporting an additive antiproliferative effect between FAM155B knockdown and paclitaxel (Fig. 7I).

Collectively, these data indicate that FAM155B contributes to paclitaxel resistance in breast cancer, and its depletion sensitizes cells to taxane-based chemotherapy both *in vitro* and *in vivo*.

Discussion

This study identifies FAM155B as a critical oncogenic driver and metabolic regulator in breast cancer. Clinical analyses revealed that elevated FAM155B expression correlates with advanced stage and poor overall survival. Functionally, FAM155B drives malignant phenotypes and accelerates tumor growth. Mechanistically, we delineated a complete regulatory axis: the chromatin remodeling factor BPTF transcriptionally activates FAM155B, which subsequently relies on SREBP1 to execute a broad lipogenic program. Importantly, this BPTF/FAM155B/SREBP1 cascade not only fuels disease progression but also orchestrates paclitaxel resistance, highlighting its dual potential as a prognostic biomarker and a therapeutic vulnerability.

Breast cancer remains a leading cause of cancer-related mortality among women [1]. Despite multimodal therapies, disease recurrence and therapeutic resistance continue to pose significant clinical challenges [4]. With the global burden projected to rise alongside socioeconomic transitions and population aging [2, 3], identifying molecular determinants that jointly govern tumor progression and drug response is imperative. In this context, the pathological overexpression of FAM155B and its correlation with adverse clinical outcomes position it as an actionable target in aggressive breast cancer subtypes.

Metabolic reprogramming is a core hallmark of cancer, enabling tumor cells to sustain unchecked proliferation and adapt to hostile microenvironments [11]. While the Warburg effect provides proliferating cells with glycolytic intermediates for anabolic processes [12–14], lipid metabolic remodeling is increasingly recognized as an equally crucial component of malignant transformation. Enhanced lipid

uptake, storage, and *de novo* lipogenesis support membrane biosynthesis, energy storage, and the generation of signaling molecules [15–17]. Consistent with these paradigms, our transcriptomic and metabolic analyses demonstrated that FAM155B acts as an upstream orchestrator of lipid anabolism, upregulating a suite of lipogenic enzymes (ACACA, FASN, SCD1, ACSL3, and DGAT1) and driving the accumulation of intracellular fatty acids, triglycerides, and lipid droplets [19].

The biological relevance of this lipogenic shift is underscored by the dependency of FAM155B-driven phenotypes on active lipid synthesis. Notably, FASN is a rate-limiting enzyme in *de novo* lipogenesis and a recognized metabolic vulnerability in cancer [18]. In our study, pharmacological blockade with FASN-IN-1 abrogated the enhanced invasive and clonogenic capacities induced by FAM155B. This confirms that enhanced lipid biosynthesis is not merely a metabolic byproduct, but an obligate downstream pathway for FAM155B-mediated oncogenesis.

Mechanistically, we identified SREBP1 as the indispensable node bridging FAM155B to this lipogenic machinery. SREBPs serve as central links connecting oncogenic signaling with lipid metabolic reprogramming [16, 19]. We observed that FAM155B selectively modulated SREBP1 while sparing SREBP2 and ChREBP. Knockdown of SREBP1 effectively neutralized the lipogenic and oncogenic advantages conferred by FAM155B, confirming that the FAM155B/SREBP1 axis is a previously uncharacterized mechanism driving breast cancer lipogenesis. Furthermore, the identification of BPTF—the largest subunit of the NURF chromatin remodeling complex—as the direct upstream transcriptional activator of FAM155B expands our understanding of how epigenetic programs dynamically reshape cancer metabolism.

A particularly clinically relevant aspect of our study is the contribution of FAM155B to paclitaxel resistance. Paclitaxel exerts its antitumor effects by stabilizing microtubules and inducing mitotic arrest [5, 6]. Resistance to paclitaxel is multifaceted, involving inflammatory pathways (e.g., IRAK1) [7], cell-cycle modulation (e.g., Lin28) [8], mitochondrial quality control (e.g., TRAP1) [9], and epigenetic remodeling (e.g., KMT5A/TWIST1) [10]. Our findings add lipid metabolic rewiring to this complex landscape. The mechanistic link between altered lipid metabolism and chemoresistance is highly plausible; enhanced lipogenesis facilitates the remodeling of lipid rafts, alters drug transporter dynamics, and buffers oxidative and endoplasmic reticulum stress during chemotherapy [20]. Strikingly, FAM155B depletion synergized with paclitaxel to profoundly suppress xenograft growth and cellular viability, suggesting that targeting this metabolic axis compromises the ability of cancer cells to withstand paclitaxel-induced cytotoxic stress.

Several limitations warrant consideration. First, while we established that FAM155B regulates SREBP1 expression, the exact molecular dynamics—whether FAM155B influences SREBP1 proteolytic processing, nuclear translocation, or protein stability—require further elucidation. Second, the epigenetic nuance of BPTF-mediated regulation, including localized histone modifications and chromatin accessibility at the FAM155B promoter, remains to be mapped. Third, our reliance on immunodeficient xenograft models precludes the evaluation of tumor-immune interactions; future studies using syngeneic

models are needed to assess how FAM155B-driven lipid accumulation affects the immune microenvironment. Finally, the predictive value of FAM155B for taxane responsiveness must be validated in larger, prospectively collected clinical cohorts.

In summary, we uncover a novel BPTF/FAM155B/SREBP1 signaling cascade that fuels lipid metabolic reprogramming, tumor progression, and chemoresistance in breast cancer. Targeting this axis, potentially in combination with taxane-based chemotherapy, offers a rational therapeutic strategy for managing metabolically aggressive and drug-resistant breast cancers.

Conclusions

In this study, we identify FAM155B as a novel oncogenic driver and metabolic regulator in breast cancer. We demonstrate that the transcription factor BPTF directly transactivates FAM155B, establishing a BPTF/FAM155B/SREBP1 signaling axis that reprograms fatty acid metabolism and thereby promotes breast cancer proliferation, metastasis, and paclitaxel resistance. These findings uncover a previously unrecognized lipid-metabolic vulnerability and suggest that targeting the FAM155B/SREBP1 axis may sensitize breast cancer cells to paclitaxel-based therapy.

Abbreviations

FAM155B: Family with sequence similarity 155 member B

BPTF: Bromodomain and PHD finger transcription factor

SREBP1: Sterol regulatory element-binding protein 1

BC: Breast cancer

TG: Triglycerides

FFA: Free fatty acids

qRT-PCR: Quantitative reverse transcription polymerase chain reaction

CCK-8: Cell Counting Kit-8

IHC: Immunohistochemistry

ChIP-qPCR: Chromatin immunoprecipitation quantitative polymerase chain reaction

shRNA: Short hairpin RNA

WT: Wild-type

MUT: Mutant

IC50: Half maximal inhibitory concentration

Declarations

Ethics approval and consent to participate

The study involving human participants was approved by the Institutional Ethics Committee of Zhongshan Hospital, Fudan University (Approval Number: B2024-237) and conducted in accordance with the Declaration of Helsinki. Informed consent was obtained from all participants. Clinical trial registration: Not applicable. All animal experiments were approved by the Animal Care and Use Committee of Zhongshan Hospital, Fudan University and performed in compliance with the ARRIVE guidelines. Mice were euthanized by carbon dioxide (CO2) inhalation in accordance with the AVMA Guidelines for the Euthanasia of Animals.

Clinical trial number

Not applicable.

Competing interests

The authors declare that they have no competing interests.

Authors' contributions

YL, SZ, and WQ contributed equally to this work and performed the experiments, data analysis, and drafted the manuscript. XZ, YF, GJ, JW, SY, WZ, and ZA participated in data collection and analysis. WZ (Wei Zhang), ZZ, and HL conceived and supervised the study and revised the manuscript. All authors read and approved the final manuscript.

Funding

This project was supported by the Fujian Provincial Natural Science Foundation of China (No. 2024J08347) and National Natural Science Foundation of China (No. 82403408 and 82403406).

Availability of data and materials

The datasets generated and analyzed during the current study are available from the corresponding author upon reasonable request.

References

1. Sung, H., et al., *Global Cancer Statistics 2020: GLOBOCAN Estimates of Incidence and Mortality Worldwide for 36 Cancers in 185 Countries*. CA Cancer J Clin, 2021. 71(3): p. 209–249.

2. Arnold, M., et al., *Current and future burden of breast cancer: Global statistics for 2020 and 2040*. Breast, 2022. 66: p. 15–23.
3. Xu, Y., et al., *Global trends and forecasts of breast cancer incidence and deaths*. Sci Data, 2023. 10(1): p. 334.
4. Waks, A.G. and E.P. Winer, *Breast Cancer Treatment: A Review.* Jama, 2019. 321(3): p. 288–300.
5. Isola, G., et al., *Periodontitis and Tooth Loss Have Negative Systemic Impact on Circulating Progenitor Cell Levels: A Clinical Study*. Genes (Basel), 2019. 10(12).
6. Weaver, B.A., *How Taxol/paclitaxel kills cancer cells*. Mol Biol Cell, 2014. 25(18): p. 2677–81.
7. Wee, Z.N., et al., *IRAK1 is a therapeutic target that drives breast cancer metastasis and resistance to paclitaxel*. Nat Commun, 2015. 6: p. 8746.
8. Lv, K., et al., *Lin28 mediates paclitaxel resistance by modulating p21, Rb and Let-7a miRNA in breast cancer cells*. PLoS One, 2012. 7(7): p. e40008.
9. Maddalena, F., et al., *Resistance to paclitxel in breast carcinoma cells requires a quality control of mitochondrial antiapoptotic proteins by TRAP1*. Mol Oncol, 2013. 7(5): p. 895–906.
10. Peng, X., et al., *Inhibition of FBP1 expression by KMT5A through TWIST1 methylation is one of the mechanisms leading to chemoresistance in breast cancer*. Oncol Rep, 2024. 52(2).
11. Hanahan, D. and R.A. Weinberg, *Hallmarks of cancer: the next generation*. Cell, 2011. 144(5): p. 646–74.
12. Pavlova, N.N. and C.B. Thompson, *The Emerging Hallmarks of Cancer Metabolism.* Cell Metab, 2016. 23(1): p. 27–47.
13. Vander Heiden, M.G., L.C. Cantley, and C.B. Thompson, *Understanding the Warburg effect: the metabolic requirements of cell proliferation*. Science, 2009. 324(5930): p. 1029–33.
14. Jiao, Y., et al., *Lanostane triterpenoids from Ganoderma curtisii and their NO production inhibitory activities of LPS-induced microglia*. Bioorg Med Chem Lett, 2016. 26(15): p. 3556–61.
15. Nolan, B.J., et al., *Beware Ketoacidosis with SGLT2 Inhibitors in Latent Autoimmune Diabetes of the Adult*. Am J Med, 2020. 133(8): p. e422–e424.
16. Cheng, C., et al., *Lipid metabolism reprogramming and its potential targets in cancer*. Cancer Commun (Lond), 2018. 38(1): p. 27.
17. Nair, H., *Role of community-based cohorts for uncovering the iceberg of disease*. Lancet Glob Health, 2021. 9(6): p. e740–e741.
18. Pizer, E.S., et al., *Pharmacological inhibitors of mammalian fatty acid synthase suppress DNA replication and induce apoptosis in tumor cell lines*. Cancer Res, 1998. 58(20): p. 4611–5.
19. Röhrig, F. and A. Schulze, *The multifaceted roles of fatty acid synthesis in cancer*. Nat Rev Cancer, 2016. 16(11): p. 732–749.
20. Beloribi-Djefaflia, S., S. Vasseur, and F. Guillaumond, *Lipid metabolic reprogramming in cancer cells*. Oncogenesis, 2016. 5(1): p. e189.

21. Saito, Y., et al., *Aldolase A promotes epithelial-mesenchymal transition to increase malignant potentials of cervical adenocarcinoma*. Cancer Sci, 2020. 111(8): p. 3071–3081.
22. Chen, S., et al., *Folate-targeted nanoparticles for glutamine metabolism inhibition enhance anti-tumor immunity and suppress tumor growth in ovarian cancer*. J Control Release, 2025. 379: p. 89–104.
23. Shin, S., et al., *Role of Nrf2 in prevention of high-fat diet-induced obesity by synthetic triterpenoid CDDO-imidazolide*. Eur J Pharmacol, 2009. 620(1–3): p. 138–44.
24. Floris, A., et al., *SUMOylation Protects FASN Against Proteasomal Degradation in Breast Cancer Cells Treated with Grape Leaf Extract*. Biomolecules, 2020. 10(4).
25. Taniguchi, M., et al., *MicroRNA-33b downregulates the differentiation and development of porcine preadipocytes*. Mol Biol Rep, 2014. 41(2): p. 1081–90.
26. Chen, M. and C. Kendziorski, *A statistical framework for expression quantitative trait loci mapping*. Genetics, 2007. 177(2): p. 761–71.
27. Francescangeli, F., M.L. De Angelis, and A. Zeuner, *Dietary Factors in the Control of Gut Homeostasis, Intestinal Stem Cells, and Colorectal Cancer*. Nutrients, 2019. 11(12).
28. Qorri, B., et al., *Next Generation of Cancer Drug Repurposing: Therapeutic Combination of Aspirin and Oseltamivir Phosphate Potentiates Gemcitabine to Disable Key Survival Pathways Critical for Pancreatic Cancer Progression*. Cancers (Basel), 2022. 14(6).

Figures

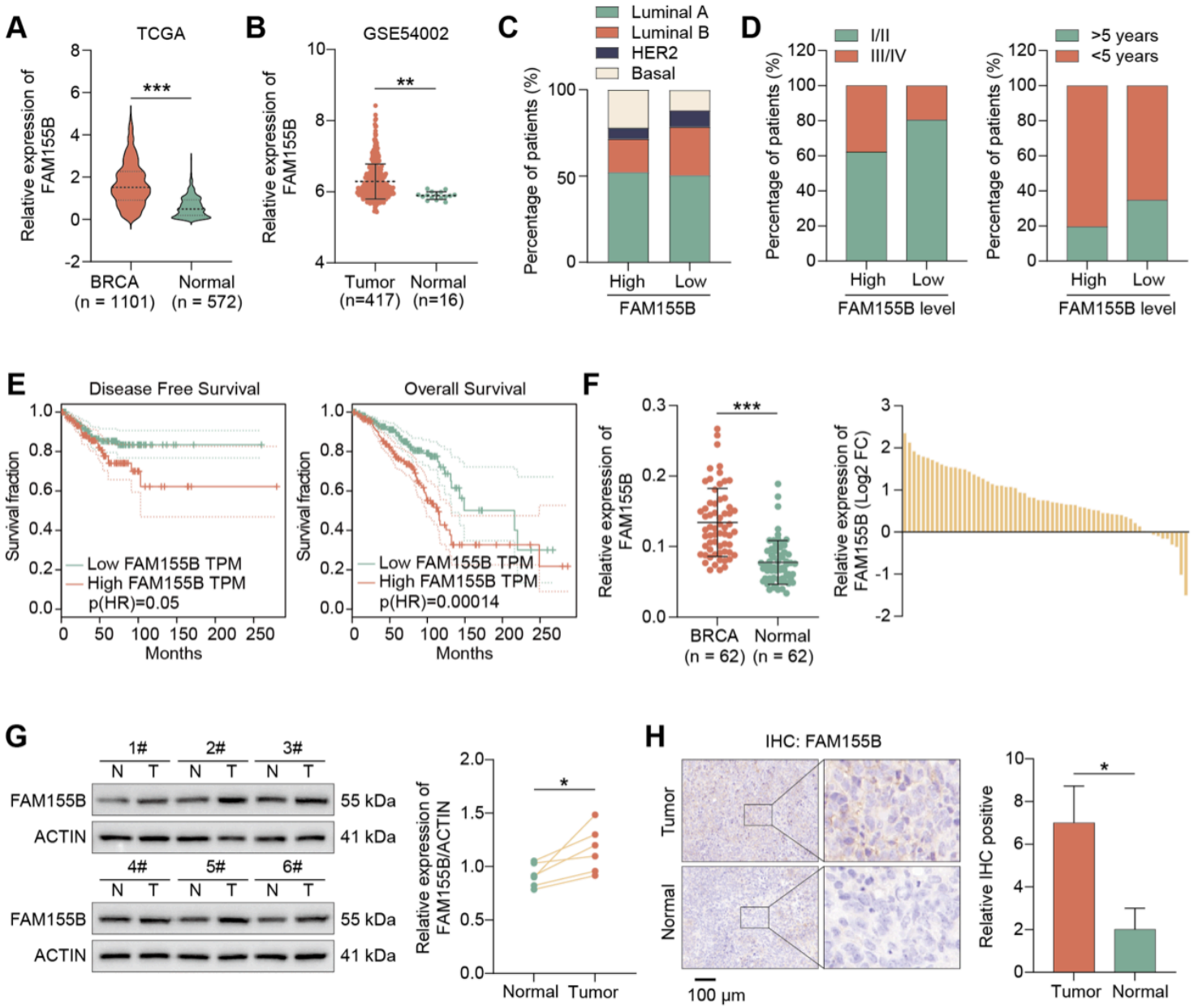


Figure 1

FAM155B is upregulated in breast cancer and correlates with clinical progression and poor prognosis. (A, B) Expression levels of FAM155B mRNA in breast cancer (BRCA) and adjacent normal tissues analyzed using the TCGA database and GSE54002 dataset. (C) Proportion of patients across different molecular subtypes (Luminal A, Luminal B, HER2, Basal) in the FAM155B-high and -low expression groups. (D) Distribution of clinical stages and 5-year survival status in the FAM155B-high and -low cohorts. (E) Kaplan-Meier curves displaying the correlation between FAM155B expression and disease-free survival or overall survival in BRCA patients. (F) Relative FAM155B mRNA expression in 62 paired BRCA and adjacent normal tissues assessed by qPCR. The waterfall plot displays the log2 fold change (FC) of FAM155B expression in individual patients. (G) Representative Western blot images of FAM155B in 6 paired BRCA (T) and adjacent normal (N) tissues. (H) Representative immunohistochemistry (IHC)

images of FAM155B staining in BRCA and normal tissues. The right graph presents the corresponding IHC scores. *Data information:* All quantitative data are presented as Mean ± SD. Statistical differences were evaluated by the log-rank test for survival analysis (E), unpaired Student's *t*-test (A, B, F left, H), and paired Student's *t*-test (G). $*p<0.05$, $**p<0.01$, $***p<0.001$.

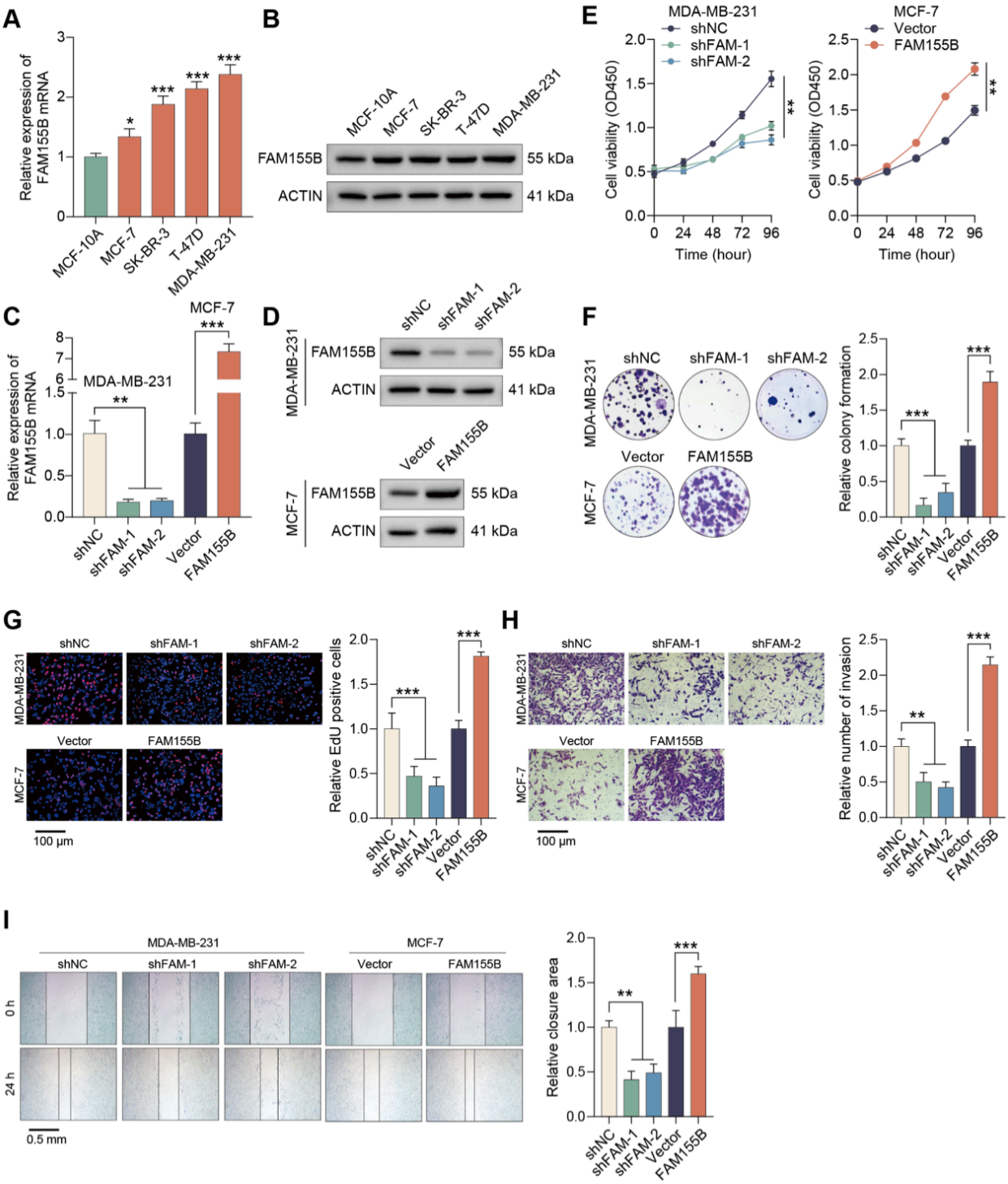


Figure 2

FAM155B promotes the proliferation, migration, and invasion of breast cancer cells in vitro. (A, B) Expression levels of FAM155B mRNA and protein in breast cancer cell lines (MCF-7, SK-BR-3, T-47D, MDA-MB-231) and normal-like breast epithelial cells (MCF-10A). (C, D) Validation of FAM155B knockdown efficiency in MDA-MB-231 cells (shFAM155B-1/2 vs. shNC) and overexpression efficiency in MCF-7 cells (FAM155B vs. Vector) at the mRNA (C) and protein (D) levels. (E) Cell viability assessed by CCK-8 assays at the indicated time points (0, 24, 48, 72, 96 hours) following FAM155B knockdown or overexpression. (F) Representative images and quantification of colony formation assays for the indicated cells. (G) Proliferation evaluated by EdU incorporation assays. (H) Cell invasion capacities measured by Transwell assays. Representative images of crystal violet-stained cells and relative quantification are presented. (I) Cell migration examined by wound healing assays. Representative images at 0 and 24 hours (left) and relative healing area quantification (right) are provided. *Data information:* All experiments were independently repeated three times (n = 3). Data are presented as Mean ± SD. Statistical differences were evaluated by one-way ANOVA followed by Tukey's post hoc test or unpaired Student's t-test. $*p<0.05$, $**p<0.01$, $***p<0.001$.

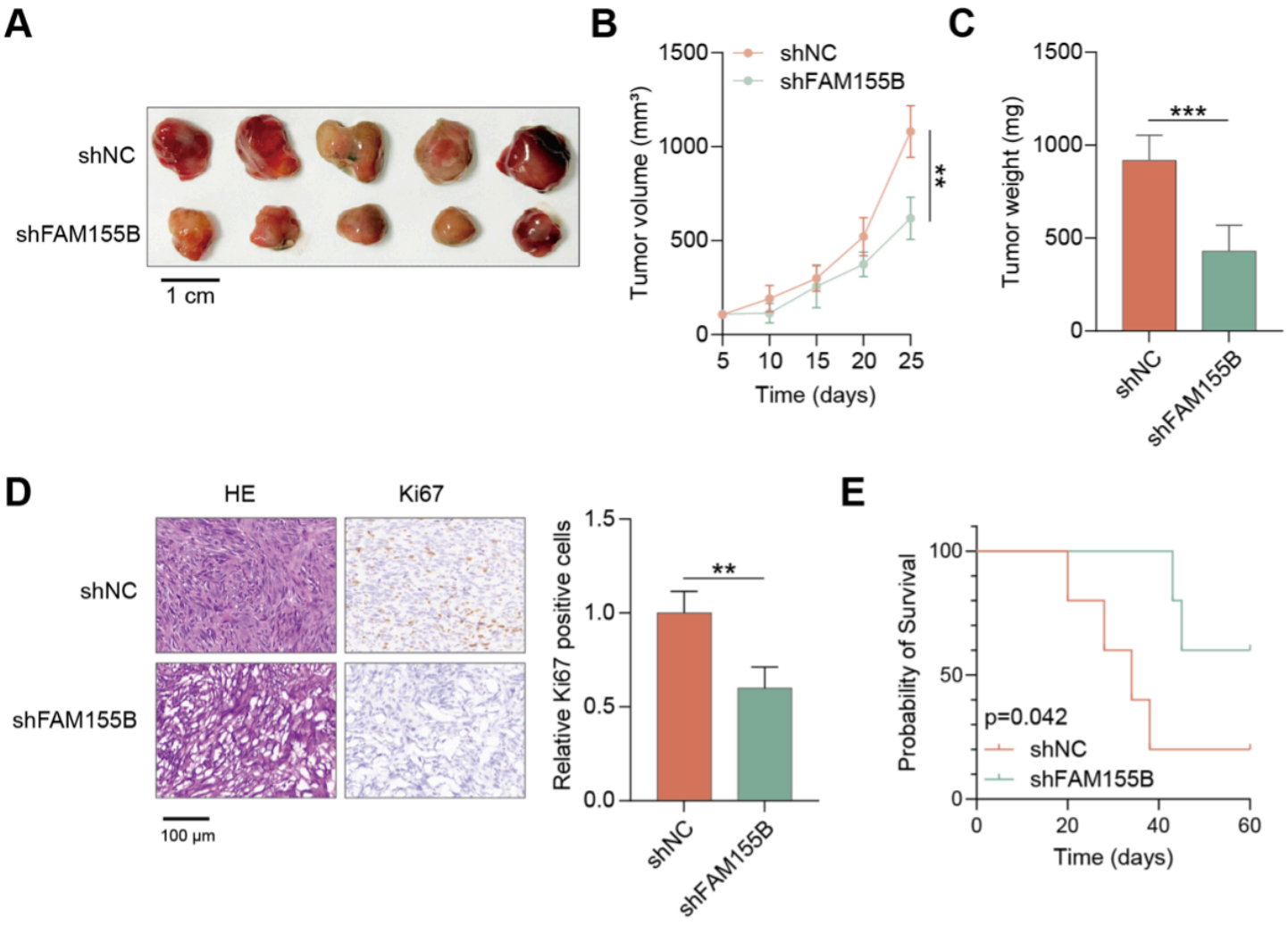


Figure 3

Knockdown of FAM155B suppresses breast cancer xenograft growth in vivo. (A) Representative images of excised tumors from the subcutaneous xenograft nude mouse model (n = 5 mice/group) at 25 days post-inoculation with MDA-MB-231 cells (shNC or shFAM155B). (B) Tumor growth curves for the indicated groups. Tumor volumes ($V=0.5\times L\times W^2$) were measured every 5 days. (C) Final tumor weights recorded at the experimental endpoint (day 25). (D) Representative images of Hematoxylin and Eosin staining and Ki67 immunohistochemical staining in tumor sections. The relative quantification of Ki67-positive cells is shown. (E) Kaplan-Meier survival curves of tumor-bearing mice (n = 5/group). The p-value was determined using the log-rank test.Data information: Quantitative data are displayed as Mean ± SD. Statistical analyses were performed by two-tailed unpaired Student's t-test (C, D) or two-way repeated measures ANOVA (B). $*p<0.05$, $**p<0.01$, $***p<0.001$.

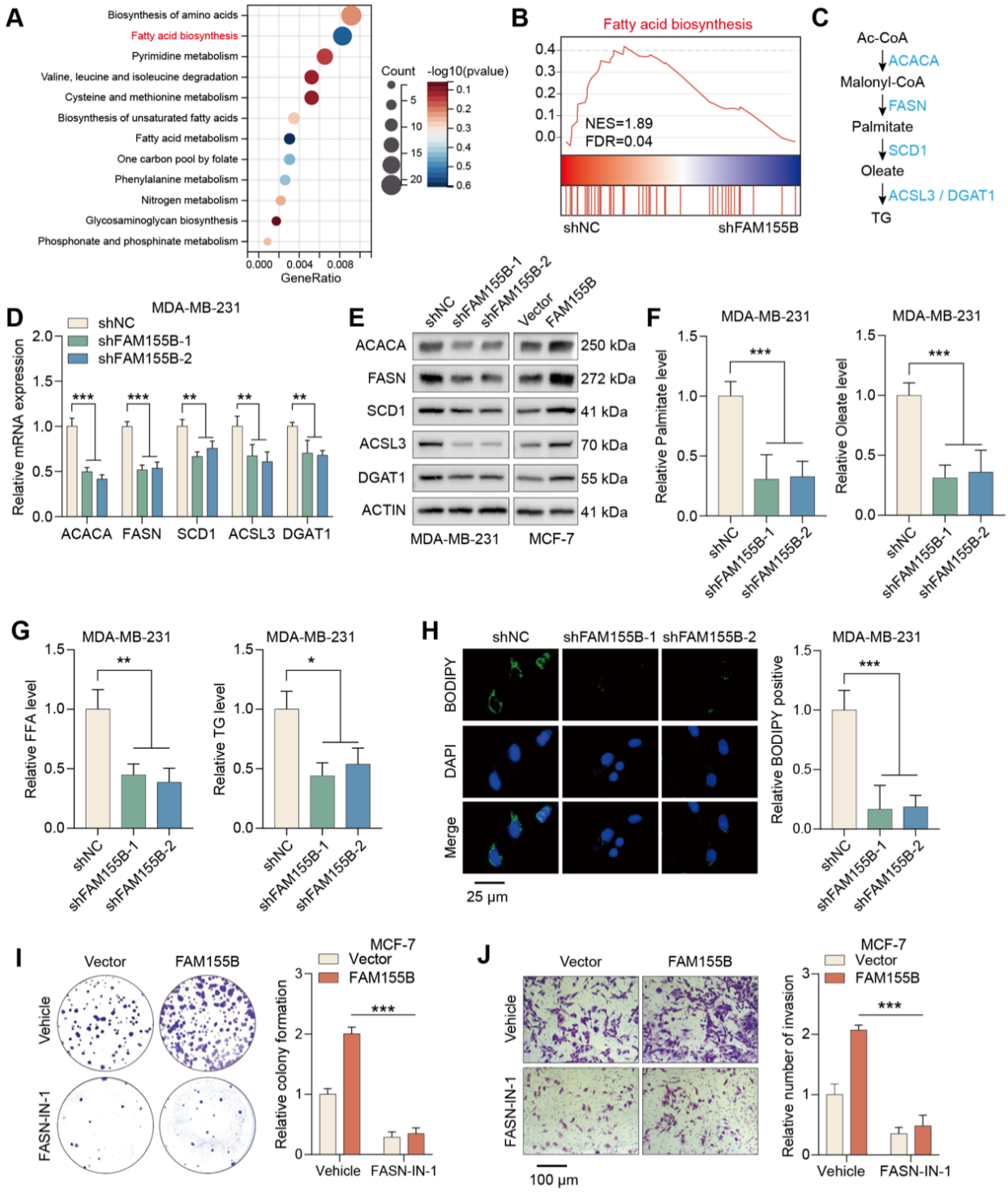


Figure 4

FAM155B promotes breast cancer progression by reprogramming fatty acid metabolism. (A, B) RNA sequencing analysis of MDA-MB-231 cells (shNC vs. shFAM155B). KEGG pathway enrichment analysis of differentially expressed genes and Gene Set Enrichment Analysis (GSEA) of the "Fatty acid biosynthesis" signature. (C) Schematic illustration of fatty acid and triglyceride (TG) biosynthesis pathways highlighting key rate-limiting enzymes. (D, E) Validation of key metabolic enzyme expressions

by qPCR and Western blot in FAM155B-knockdown MDA-MB-231 cells and FAM155B-overexpressing MCF-7 cells. (F, G) Relative intracellular concentrations of palmitate and oleate, and total free fatty acids (FFA) and triglycerides (TG) in MDA-MB-231 cells upon FAM155B depletion. (H) Representative fluorescence images of BODIPY 493/503 staining and corresponding quantification displaying lipid droplet accumulation. (I, J) Rescue effects of pharmacological FASN inhibition. FAM155B-overexpressing MCF-7 cells were treated with a FASN inhibitor (FASN-IN-1, 10 μM). Representative images and quantifications of colony formation and Transwell invasion assays are shown. Data information: In vitro experiments were repeated at least 3 times. Data are represented as Mean ± SD. Statistics were derived using Student's t-test or one-way ANOVA. $*p<0.05$, $**p<0.01$, $***p<0.001$.

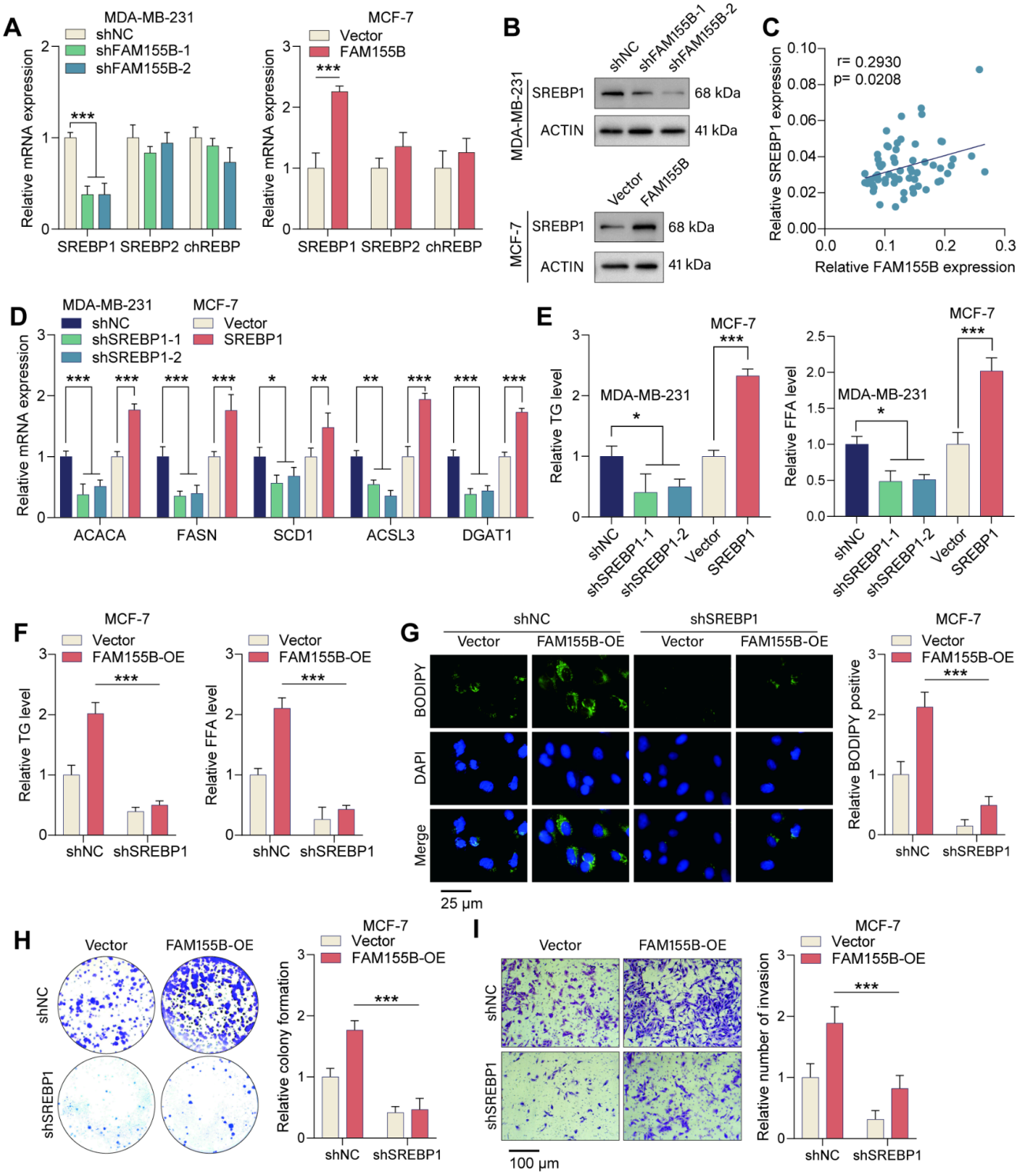


Figure 5

FAM155B mediates lipid metabolic reprogramming and oncogenic phenotypes via the transcription factor SREBP1.(A, B) Expression of lipogenic transcription factors (SREBP1, SREBP2, ChREBP) measured by qPCR and Western blot in FAM155B genetically modified cells, indicating specific regulation of SREBP1. (C) Correlation between the mRNA levels of FAM155B and SREBP1 in clinical patient samples. (D, E) Impact of altered SREBP1 expression on downstream metabolic enzymes and

intracellular total TG and FFA levels. (F-I) Functional rescue assays. Concurrent SREBP1 knockdown and FAM155B overexpression reversed the increases in TG/FFA and lipid droplet accumulation, and significantly abrogated FAM155B-driven colony formation and cell invasion capacities. Data information: Data are shown as Mean ± SD (n = 3). Statistical evaluation used Student's t-test or one-way ANOVA. ∗p<0.05, ∗∗p<0.01, ∗∗∗p<0.001.

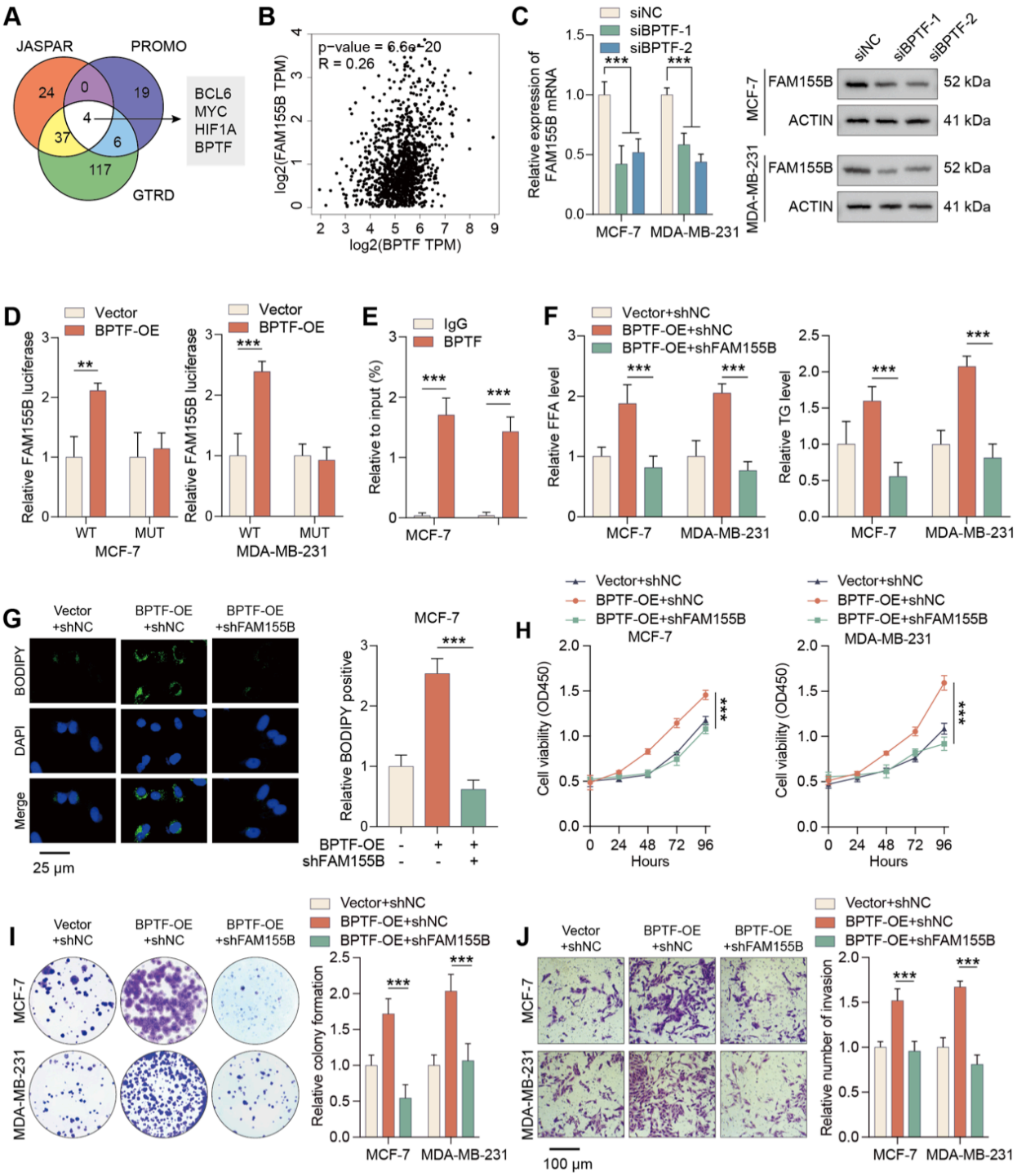


Figure 6

BPTF acts as an upstream transcriptional activator of FAM155B to promote lipid metabolic reprogramming. (A) Intersection of candidate transcription factors predicted to bind the FAM155B promoter across JASPAR, PROMO, and GTRD databases. (B) Correlation between the mRNA expression of BPTF and FAM155B based on public databases. (C) FAM155B transcript and protein expression profiles following BPTF knockdown in MCF-7 and MDA-MB-231 cells. (D) Relative luciferase activities of wild-type (WT) or mutant (MUT) FAM155B promoters in cells overexpressing BPTF. (E) ChIP-qPCR analysis showing BPTF enrichment at the FAM155B promoter region against IgG control. (F-J) Rescue experiments evaluating the dependencies of BPTF-induced alterations. Concurrent FAM155B knockdown largely abrogated BPTF-enhanced FFA and TG accumulation, lipid droplet formation, cell proliferation via CCK-8, colony formation, and cell invasion. Data information: Data are expressed as Mean ± SD (n = 3). Significance was determined via Student's t-test or one-way ANOVA. ∗p<0.05, ∗∗p<0.01, ∗∗∗p<0.001.

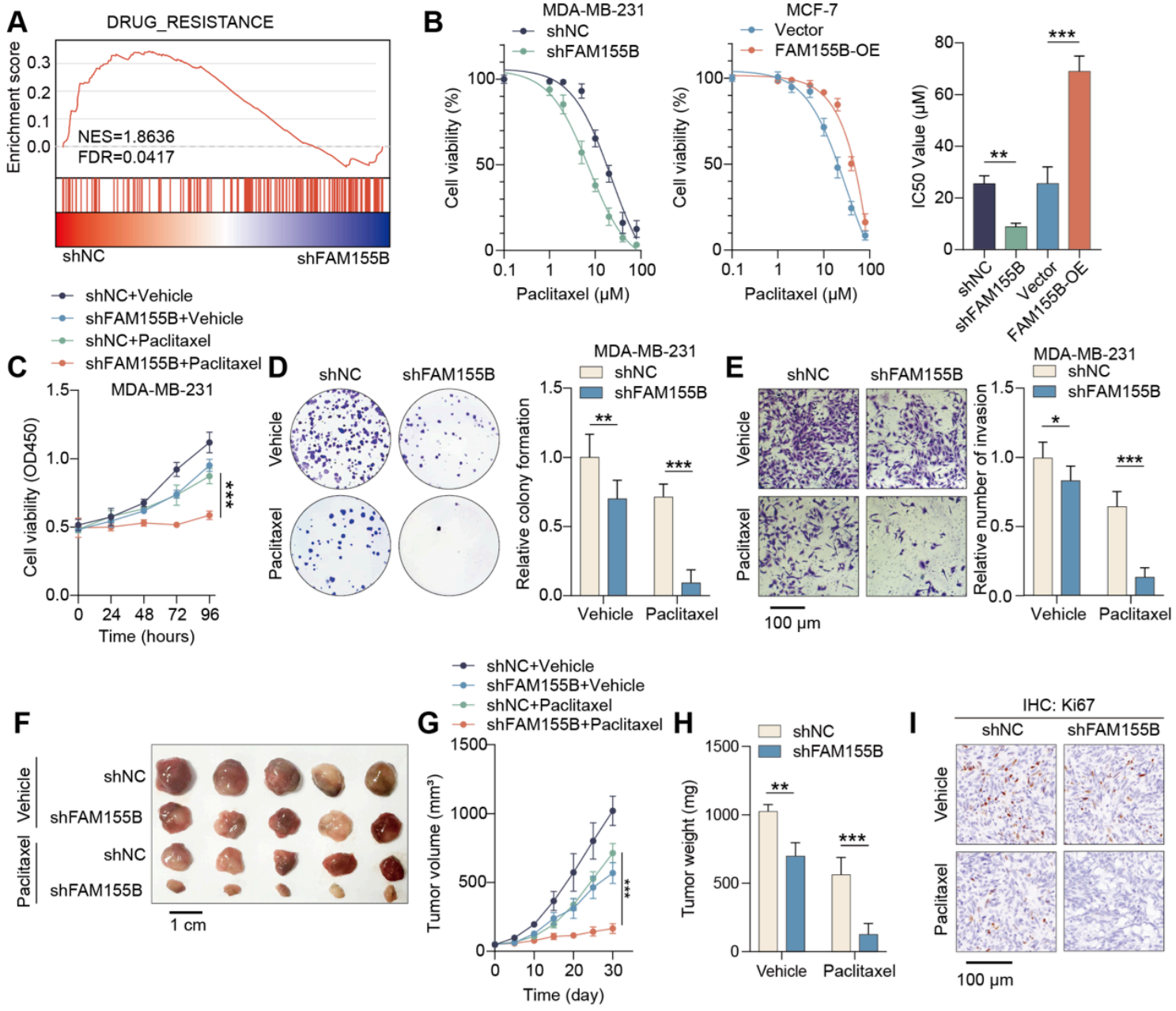


Figure 7

FAM155B silencing sensitizes breast cancer cells to paclitaxel treatment in vitro and in vivo. (A) GSEA showing significant enrichment of drug resistance-associated signatures in shFAM155B cells relative to shNC cells. (B) Dose-response cytotoxicity curves and calculated IC50 values for MDA-MB-231 and MCF-7 cells under varying paclitaxel concentrations. (C-E) Efficacy of paclitaxel in combination with FAM155B depletion on MDA-MB-231 short-term cell viability, long-term colony formation capability, and cell invasion. (F) Representative images of excised subcutaneous tumors from different pharmacological and genetic treatment groups. (G, H) In vivo tumor growth curves and final tumor weights indicating an enhanced anti-tumor efficiency upon paclitaxel administration combined with FAM155B silencing (n = 5 mice/group). (I) Representative IHC images of Ki67 in the xenograft tumors across treatment groups. Data information: In vitro data are Mean ± SD (n\ge 3). Statistical comparisons utilized nonlinear regression (IC50), two-way ANOVA, one-way ANOVA, or Student's t-test appropriately. $*p<0.05$, $**p<0.01$, $***p<0.001$.

Supplementary Files

This is a list of supplementary files associated with this preprint. Click to download.

- SupplementFigure.docx